JOURNAL OF GUIDANCE, CONTROL, AND DYNAMICS
Vol. 17, No. 6, November–December 1994

# Aeroelastic Vehicle Multivariable Control Synthesis with Analytical Robustness Evaluation

Brett Newman*
*Old Dominion University, Norfolk, Virginia 23529-0247*
and
David K. Schmidt†
*University of Maryland, College Park, Maryland 20742-3015*

**The vehicle to be augmented is representative of a large, high-speed transport, with first fuselage aeroelastic mode frequency at 6 rad/s, very close to the 2 rad/s short-period mode. An integrated flight and aeroelastic mode control law is synthesized using a previously developed model-following synthesis approach. This technique, designed to yield desired closed-loop rather than open-loop shapes, involves a specific linear quadratic regulator (LQR) formulation leading to the model-following state feedback gains. Then the use of asymptotic loop transfer recovery is utilized to obtain the compensation that recovers the LQR robustness properties and leads to an output feedback control law. A conventionally designed control law is also developed for comparison purposes. The resulting closed-loop systems are then evaluated in terms of their performance and multivariable stability robustness, measured in terms of the appropriate singular values. This evaluation includes the use of approximate analytical expressions for those singular values, expressed in terms of analytical expressions for the poles and zeros appearing in the vehicle transfer function matrix. It is found that the control laws possess roughly equivalent performance and stability robustness, and the characteristics limiting this robustness are traced to some specific loop gains and the frequency and damping of the open-loop aeroelastic mode dipole. Furthermore, closed-form analytical expressions for these characteristics are presented in terms of the stability derivatives of the vehicle. Insight from such an analysis would be hard to obtain from a strictly numerical procedure.**

## Introduction

THE supersonic and hypersonic capabilities of advanced aerospace vehicles and the use of extremely light metallic or composite materials in the vehicle structure can lead to vehicles with significant dynamic coupling between the rigid-body and elastic motions. References 1 and 2, for example, specifically address this coupling at the earliest stage of system modeling and flight control synthesis.

Augmentation of an aeroelastic vehicle's open-loop dynamics via feedback is often necessary to provide sufficient levels of stability and performance (e.g., handling qualities). Feedback is used to stabilize the attitude and/or aeroelastic responses (such as static aerodynamic instability or flutter) or just augment damping. Crossfeeds may also be used to improve the dynamic responses. Further, the control law must ensure this stability and performance in the presence of vehicle modeling errors (i.e., robustness). For aeroelastic vehicle applications, modeling errors can arise from uncertainty in the aerodynamic model and neglected high-frequency structural modes, both leading to uncertainty in the pole/zero locations in the vehicle transfer functions, for example. Such control objectives have been noted in the literature.[3–8]

If possible, the vehicle model (used in control synthesis) should aid in the understanding and thereby provide insight regarding the vehicle physics, exposing key dynamic characteristics and their causes. This can be achieved by developing analytical expressions for the vehicle transfer functions (gains, zeros, and poles) in terms of vehicle model parameters, such as stability and control derivatives or vibrational characteristics, which have their genesis in the fundamental vehicle geometric shape and structural layout.[2,9–13] Models of this type can be an extremely valuable tool in open-loop or closed-loop design.

The control synthesis for an aeroelastic vehicle, and the analysis thereof, specifically using an analytical model, is the subject of this paper.[14] An aeroelastic vehicle model is briefly presented and deficiencies in the vehicle dynamics are noted. A new approach to model-following control synthesis[15] is briefly discussed and applied to the vehicle model. A conventional or classical control synthesis approach is also considered for the purposes of comparison. The resulting compensators and closed-loop systems are analyzed with an analytical model to expose sources of system characteristics that limit the closed-loop system stability robustness. It will be shown, for example, that major among these critical characteristics are the frequency and damping of the vehicle first aeroelastic mode dipole, and closed-form expressions for these terms are presented as functions of the vehicle stability derivatives and vibrational characteristics.

## Vehicle Modeling for Feedback Synthesis

The configuration to be considered is a large, high-speed aircraft of reasonably conventional geometry with a low-aspect-ratio swept wing, conventional tail, and canard.[2,10,11] Controlled inputs consist of elevator deflection $\delta_E$ and canard (located near the cockpit) deflection $\delta_C$. The reference flight condition is level flight at Mach 0.6 and altitude 5000 ft.

The complete nonlinear modeling of this vehicle was the subject of Ref. 2, and the development of low-order linear models for control synthesis was considered in Refs. 10 and 11. A fourth-order state-space realization and the corresponding transfer functions for this linear model are given in Tables 1 and 2. This model involves the small-perturbation longitudinal dynamics of the closely spaced, effective short-period and first aeroelastic modes. The responses of interest are the rigid-body angle of attack $\alpha$, rigid-body pitch rate $q$, and pitch rate $q'$ measured at the cockpit. Here, rigid-body $\alpha$ and $q$ are the angle of attack and pitch rate associated with the vehicle mean axes. An approximate measurement of $q$ can be obtained from a rate gyro located at the antinode of the first elastic structural mode, followed with low-pass filtering of the higher frequency structural

Presented as Paper 90-3446 at the AIAA Guidance, Navagation, and Control Conference, Portland, OR, Aug. 20–22, 1990; received Sept. 15, 1992; revision received Jan. 26, 1994; accepted for publication April 5, 1994. 

*Assistant Professor, Department of Aerospace Engineering. Member AIAA.

†Chairman and Professor, Department of Aerospace Engineering. Associate Fellow AIAA.

**Table 1 Elastic aircraft state-space model**

$$\dot{x}(t) = Ax(t) + Bu(t)$$

$$y(t) = Cx(t)$$

$$y = \begin{bmatrix} \alpha \text{ (rad)} \\ q \text{ (rad/s)} \\ q' \text{ (rad/s)} \end{bmatrix} \qquad u = \begin{bmatrix} \delta_E \text{ (rad)} \\ \delta_C \text{ (rad)} \end{bmatrix}$$

$$A = \begin{bmatrix} -0.517 & 3.85 & 0.150 & 4.24 \\ -9.39 & -0.318 & -0.523 & -4.67 \\ 0.0438 & 0.0164 & -0.0128 & -2.06 \\ -0.0591 & -0.0165 & 0.764 & -0.986 \end{bmatrix}$$

$$B = \begin{bmatrix} -292 & -182 \\ -598 & -424 \\ 53.7 & -31.2 \\ -38.4 & 17.7 \end{bmatrix}$$

$$C = \begin{bmatrix} 0.000480 & -0.0000247 & -0.0188 & -0.0286 \\ 0.00147 & 0.00170 & -0.0264 & 0.0549 \\ -0.0222 & -0.0213 & -0.0372 & 0.0687 \end{bmatrix}$$

**Table 2 Elastic aircraft transfer functions**

| | | |
|---|---|---|
| $\frac{\alpha(s)}{\delta_E(s)}$ | $= \frac{-0.036(s - 0.018 \pm j4.9)(s + 150)}{d(s)}$ | (rad/rad) |
| $\frac{q(s)}{\delta_E(s)}$ | $= \frac{-5.0(s + 0.36)(s + 0.11 \pm j4.9)}{d(s)}$ | (rad/s/rad) |
| $\frac{q'(s)}{\delta_E(s)}$ | $= \frac{15.(s + 0.040)(s - 2.9)(s + 4.0)}{d(s)}$ | (rad/s/rad) |
| $\frac{\alpha(s)}{\delta_C(s)}$ | $= \frac{0.0044(s + 1.8 \pm j9.0)(s + 200)}{d(s)}$ | (rad/rad) |
| $\frac{q(s)}{\delta_C(s)}$ | $= \frac{0.80(s + 0.33)(s + 1.3 \pm j9.1)}{d(s)}$ | (rad/s/rad) |
| $\frac{q'(s)}{\delta_C(s)}$ | $= \frac{15.(s + 0.056)(s + 0.73 \pm j2.9)}{d(s)}$ | (rad/s/rad) |
| $d(s)$ | $= (s + 0.47 \pm j1.2)(s + 0.44 \pm j6.0)$ | |

dynamics. The effects of such filtering will not be specifically addressed, but it would add additional phase loss in the loops, which is considered in the robustness analysis.

The fourth-order model was developed to accurately approximate the appropriate frequency responses of a twelfth-order model in the anticipated critical frequency range of 1–10 rad/s. Figures 1–3 show some of the open-loop (vehicle-only) frequency responses excited by the elevator. Note that the next significant unmodeled aeroelastic mode lies just beyond the region of interest at 11 rad/s. From Table 2 and Figs. 1–3, the major open-loop dynamic deficiency is the level of damping of the short-period and aeroelastic modes. Furthermore, the aeroelastic mode contributes significantly to the vehicle's dynamic responses. Figures 1–3 also contain the closed-loop frequency responses excited by the pilot stick input $\delta$, a blend of elevator and canard, the development of which is considered next.

## Classical Control Synthesis

A conventional design approach will be considered here, consisting of sequential single-loop closures, using root loci, and relying upon knowledge of the physics of the elastic aircraft for synthesis strategy. Consider a 2 × 2 system from Table 2 with the following notation:

$$q(s) = g_{11}(s)\delta_E(s) + g_{12}(s)\delta_C(s)$$
$$q'(s) = g_{21}(s)\delta_E(s) + g_{22}(s)\delta_C(s) \qquad (1)$$

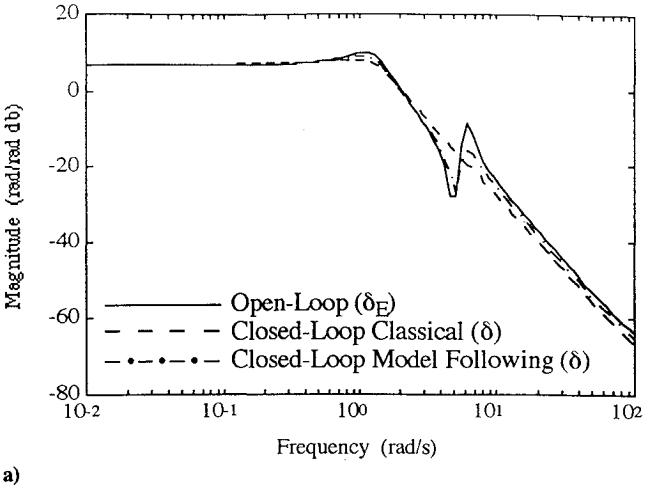


a)

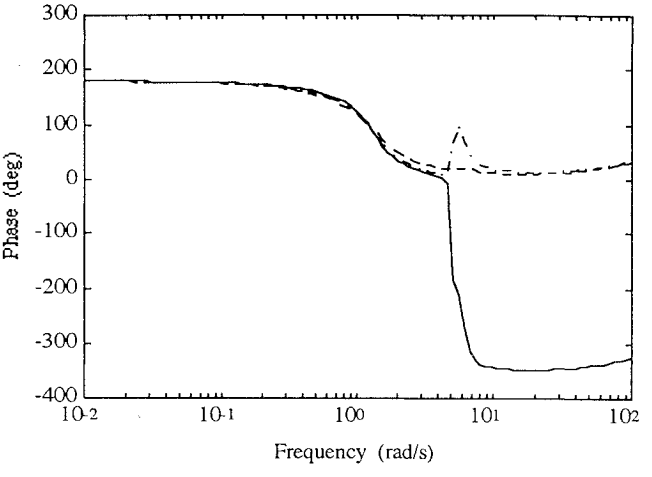


b)

**Fig. 1 Angle-of-attack frequency responses.**

First, the $q'/\delta_C$ loop is closed to improve the aeroelastic mode damping. Recall that $q'$ and $\delta_C$ correspond to a colocated sensor and actuator pair near the cockpit. The control law $\delta_C = \delta'_C - k_{22}q'$ yields

$$q = \left(g_{11} - \frac{k_{22}g_{12}g_{21}}{1 + k_{22}g_{22}}\right)\delta_E + g_{12}\left(1 - \frac{k_{22}g_{22}}{1 + k_{22}g_{22}}\right)\delta'_C$$
$$q' = \frac{g_{21}}{1 + k_{22}g_{22}}\delta_E + \frac{g_{22}}{1 + k_{22}g_{22}}\delta'_C \qquad (2)$$

The root locus for $1 + k_{22}(n_{22}/d)$, where $n_{ij}$ and $d$ are the numerator and denominator polynomials, respectively, of $g_{ij}$, is shown in Fig. 4. A gain of $k_{22} = 0.05$ rad/rad/s increases the aeroelastic mode damping by over 60% of the open-loop value.

An elevator-to-canard crossfeed is now introduced to reduce aeroelastic mode excitation from the elevator. Interconnecting "up canard" with "up elevator" will reduce aeroelastic mode deflections from the elevator because the fuselage mode shape is similar to the fundamental bending mode shape of a slender beam.[2]

The crossfeed $\delta'_C = k_{cf}\delta_E$ yields

$$q = \frac{g_{11} + k_{22}(g_{11}g_{22} - g_{12}g_{21}) + k_{cf}g_{12}}{1 + k_{22}g_{22}}\,\delta_E \qquad (3)$$

This can be simplified with the identity[7]

$$\det[G] = \det\begin{bmatrix} g_{11} & g_{12} \\ g_{21} & g_{22} \end{bmatrix} = g_{11}g_{22} - g_{12}g_{21} = \frac{\psi_G}{d} \qquad (4)$$

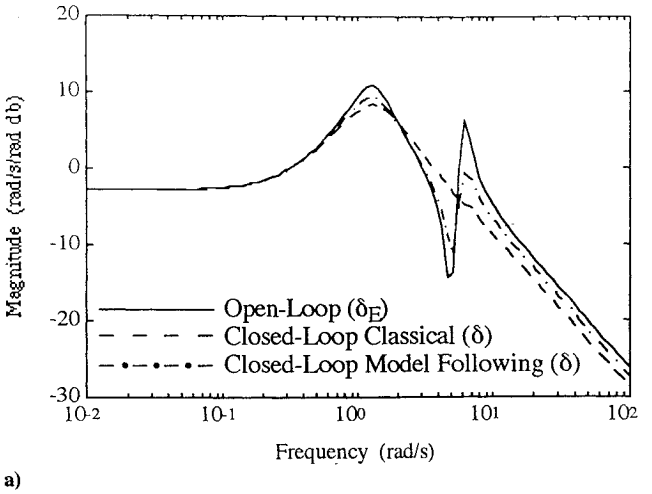


a)

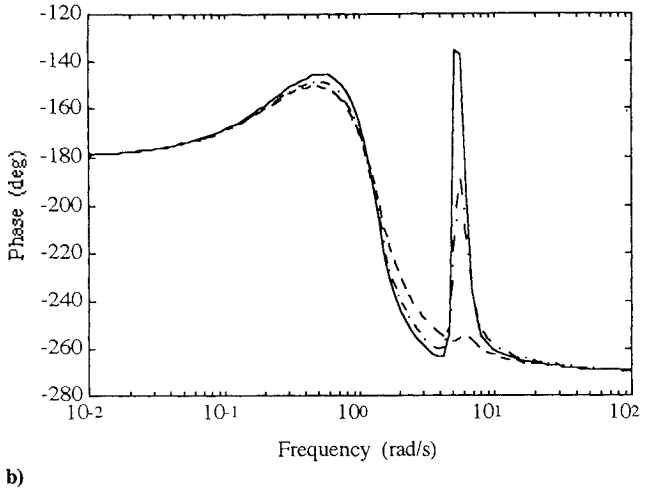


b)

**Fig. 2 Rigid-body pitch rate frequency responses.**

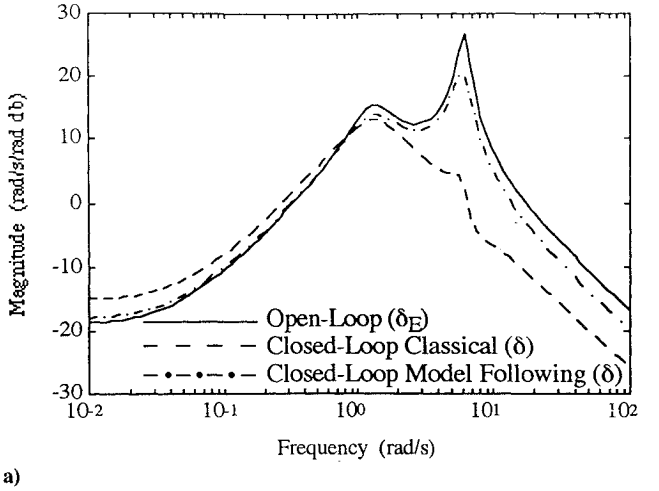


a)

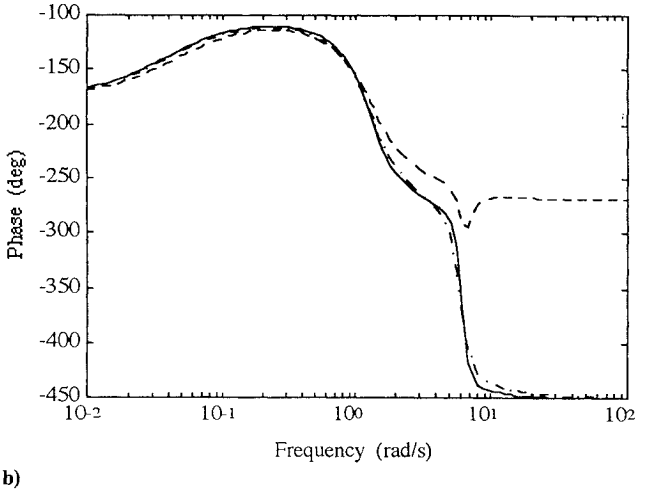


b)

**Fig. 3 Cockpit pitch rate frequency responses.**

where $G$ represents the plant transfer function matrix corresponding to Eq. (1) and $\psi_G$ is the transmission zero polynomial corresponding to $G$:

$$\psi_G(s) = -89(s + 0.081)(s + 0.46) \tag{5}$$

Substitution of Eq. (4) into Eq. (3) yields

$$q = \frac{n_{11} + k_{22}\psi_G + k_{cf}n_{12}}{d + k_{22}n_{22}}\delta_E \tag{6}$$

Observe from Eq. (6) that the crossfeed has the effect of moving the zeros of the $q/\delta_E$ transfer function (with the $q'/\delta_C$ loop closed) from $n_{11} + k_{22}\psi_G$ to $n_{12}$. The root locus for $1 + k_{cf}(n_{12}/(n_{11} + k_{22}\psi_G))$ is shown in Fig. 5. A gain of $k_{cf} = -1.5$ rad/rad results in almost perfect pole-zero cancellation for the aeroelastic dipole in the effective $q/\delta_E$ transfer function.

Finally, the effective $q/\delta_E$ loop is closed to further improve the short-period damping. The control law $\delta_E = p\delta - k_{11}q$ yields

$$q = \frac{p[g_{11} + k_{22}(g_{11}g_{22} - g_{12}g_{21}) + k_{cf}g_{12}]}{1 + k_{22}g_{22} + k_{11}[g_{11} + k_{22}(g_{11}g_{22} - g_{12}g_{21}) + k_{cf}g_{12}]}\delta \tag{7}$$

where $p$ is the gain on the pilot input $\delta$. The root locus for $1 + k_{11}((n_{11} + k_{22}\psi_G + k_{cf}n_{12})/(d + k_{22}n_{22}))$ is shown in Fig. 6, as well as the final closed-loop pole locations for a gain of $k_{11} = -0.05$ rad/rad/s. A value of $p = 0.6$ rad/rad was chosen to adjust the closed-loop frequency response direct-current (DC) value to that of the open-loop system excited by the elevator.

With some block-diagram manipulation, the closed-loop system can be represented as in Fig. 7. Observe that pilot input results in a blend of elevator and canard deflections. Table 3 contains the effective closed-loop transfer functions corresponding to the pilot command $\delta$, whereas Figs. 1–3 show the corresponding frequency responses for the augmented vehicle. Short-period damping has improved from $\zeta_{sp} = 0.36$ (see Table 2) to $\zeta_{sp} = 0.54$ (a 50% increase), whereas the first aeroelastic mode damping has improved from $\zeta_{f_1} = 0.073$ (see Table 2) to $\zeta_{f_1} = 0.12$ (a 64% increase). These improvements are apparent in the closed-loop frequency responses.

Significant improvement in the rigid-body ($\alpha$ and $q$) frequency response shapes is also achieved. Besides improved short-period damping, the aeroelastic mode pole-zero "sawtooth" shapes located near 6 rad/s in Figs. 1 and 2 are virtually eliminated when compared to the corresponding open-loop behavior. This is a result of improved closed-loop pole-zero cancellations (see Table 3), as desired in the conventional control synthesis, or the aeroelastic mode has been rendered undisturbable from pilot input.

## Model-Following Control Synthesis

A newly developed technique for the synthesis of flight control laws will now be outlined.[15] Although linear quadratic regulator (LQR) and loop transfer recovery (LTR) concepts are used in the formulation of the algorithm, this approach is fundamentally different from LQR/LTR methodology.[4] LQR/LTR address the problem of obtaining specified open-loop shapes, whereas the approach taken here is to synthesize a control law that yields a desired closed-loop shape.

The system to be controlled is represented as

$$\dot{x}(t) = Ax(t) + Bu(t) \qquad y(t) = Hx(t) \tag{8}$$

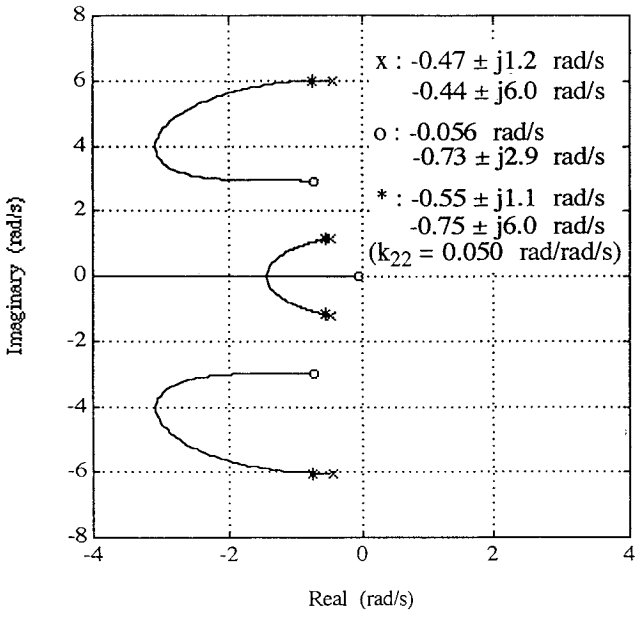


**Fig. 4 Cockpit pitch-rate-to-canard root locus.**

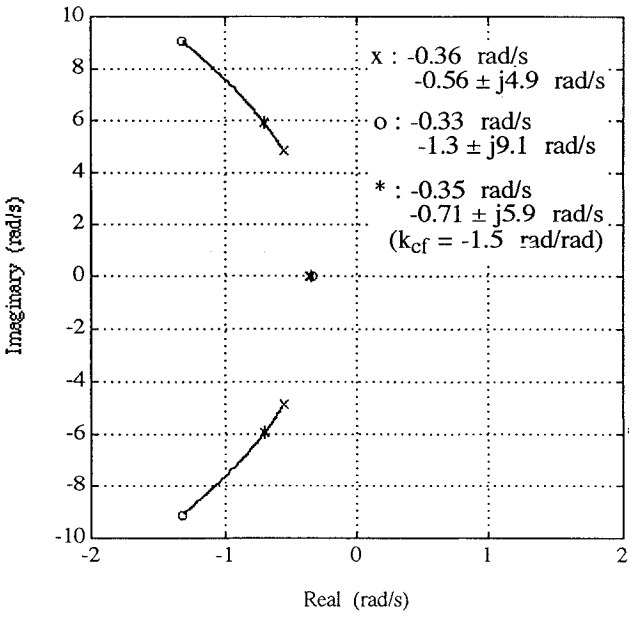


**Fig. 5 Elevator-to-canard root locus.**

and the model of the desired dynamics to be followed is

$$\begin{aligned} \dot{x}_m(t) &= A_m x_m(t) + B_m \delta(t) \\ y_m(t) &= H_m x_m(t) \\ \dot{\delta}(t) &= -100\delta(t) \end{aligned} \tag{9}$$

where $\delta$ represents the input from the pilot. The error vector

$$e(t) = y(t) - y_m(t) \tag{10}$$

is constrained to be governed by stable, homogeneous dynamics

$$\dot{e}(t) = -Ge(t) \tag{11}$$

where $G$ is to be selected in the synthesis process. The model-following control law is obtained by solving the LQR problem with the following objective function:

$$J = \int_0^\infty [(\dot{e} + Ge)^T Q(\dot{e} + Ge) + u^T R u]\, \mathrm{d}t \tag{12}$$

If the product $HB$ is square and invertible, and the same for $H_m$, and if $G$ is chosen as $G = -H_m A_m H_m^{-1}$, then perfect model following is achieved asymptotically as $R$ in Eq. (12) approaches the null matrix. If this is the case, then the closed-loop poles approach both the *desired model poles* (for $G$ as defined above) and any *open-loop plant finite transmission zeros* (or their stable mirror image).[15] The solution to this problem is the first step of the control law synthesis, yielding the state-feedback control law

$$u = -Kx - K_\delta \delta \tag{13}$$

For the elastic aircraft model in Table 1, rigid-body angle of attack and pitch rate $\alpha$ and $q$ are selected as responses for model following. This allows the handling characteristics to be augmented more toward that of a rigid vehicle. Also, with this selection, the open-loop plant transmission zeros are located at $-23$ and $35\ \mathrm{s}^{-1}$, and $HB$ is square and invertible. Note $H$ consists of the first two rows of $C$ from Table 1.

The model of the desired dynamics is chosen to be

$$\begin{aligned} \frac{\alpha_m(s)}{\delta(s)} &= \frac{-3.5}{s + 0.89 \pm j0.91} \\ \frac{q_m(s)}{\delta(s)} &= \frac{-3.3(s + 0.36)}{s + 0.89 \pm j0.91} \end{aligned} \tag{14}$$

which represents a well-damped short-period mode. With this selection, $H_m$ is square and also invertible. Observe that the system to be controlled is fourth order, whereas the desired dynamics are second order. Therefore, as $R$ in Eq. (12) asymptotically approaches the null matrix, the short-period poles will approach those of the model, and the aeroelastic mode poles will move toward the plant transmission zeros (or their stable mirror images, i.e., $-23$ and $-35\ \mathrm{s}^{-1}$). Further, the $\alpha$ and $q$ time and frequency responses will be shaped to better approximate those of a rigid vehicle. Figure 8 shows this closed-loop pole loci behavior as the scalar parameter $\rho$ is decreased with

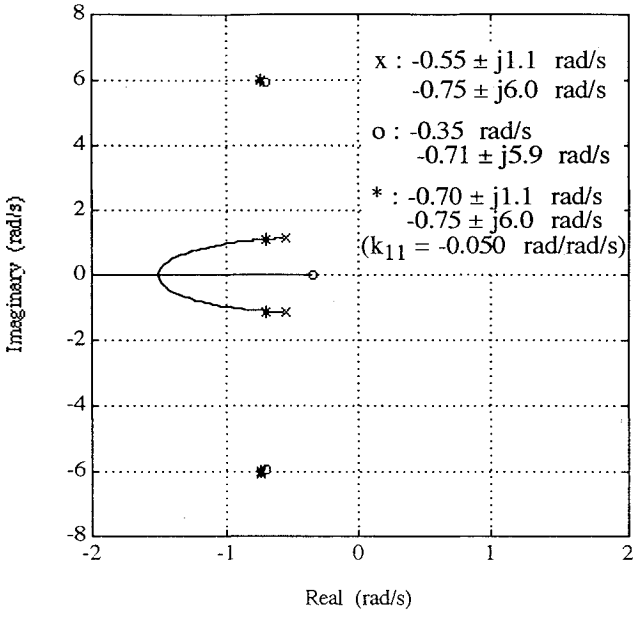


**Fig. 6 Rigid-body pitch-rate-to-elevator root locus.**

$$Q = \begin{bmatrix} 1\ \mathrm{s}^2/\mathrm{rad}^2 & 0 \\ 0 & 1\ \mathrm{s}^4/\mathrm{rad}^2 \end{bmatrix} \qquad R = \rho \begin{bmatrix} 1\ \mathrm{rad}^{-2} & 0 \\ 0 & 1\ \mathrm{rad}^{-2} \end{bmatrix} \tag{15}$$

A value of $\rho = 70$ increases the short-period and aeroelastic mode damping by over 20% and 60%, respectively.

With the state-feedback gains $K$ and $K_\delta$ so determined, compensators will now be synthesized using the loop transfer recovery procedure,[4] which will then yield an output feedback loop structure rather than a state-feedback structure. Although the $\alpha$ and $q$ responses were used in the model-following step, they are not the

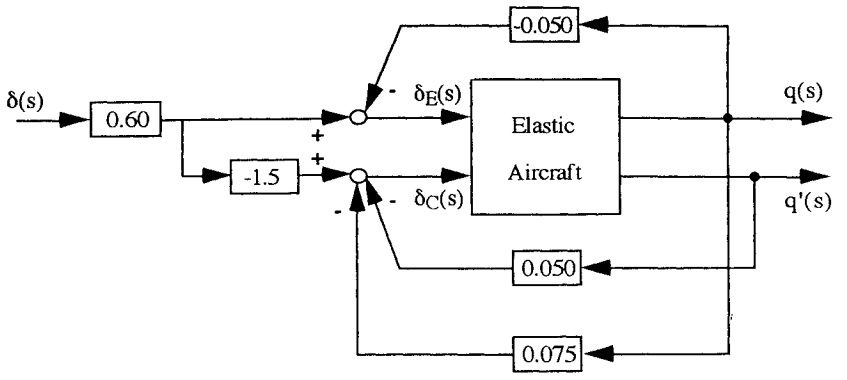


**Fig. 7 Classically designed closed-loop system.**

**Table 3 Closed-loop transfer functions**

Classical synthesis

$$\frac{\alpha(s)}{\delta(s)} = \frac{-0.025(s+0.70\pm j5.9)(s+160)}{d(s)} \quad \text{(rad/rad)}$$

$$\frac{q(s)}{\delta(s)} = \frac{-3.7(s+0.35)(s+0.71\pm j5.9)}{d(s)} \quad \text{(rad/s/rad)}$$

$$\frac{q'(s)}{\delta(s)} = \frac{-5.1(s+0.049)(s+1.0\pm j6.6)}{d(s)} \quad \text{(rad/s/rad)}$$

$$d(s) = (s+0.70\pm j1.1)(s+0.75\pm j6.0)$$

Model-following synthesis

$$\frac{\alpha(s)}{\delta(s)} = \frac{-0.0062(s+0.22\pm j5.1)(s+150)}{d(s)} \quad \text{(rad/rad)}$$

$$\frac{q(s)}{\delta(s)} = \frac{-0.87(s+0.36)(s+0.34\pm j5.1)}{d(s)} \quad \text{(rad/s/rad)}$$

$$\frac{q'(s)}{\delta(s)} = \frac{2.0(s+0.042)(s-3.6)(s+4.5)}{d(s)} \quad \text{(rad/s/rad)}$$

$$d(s) = (s+0.56\pm j1.1)(s+0.73\pm j5.8)$$

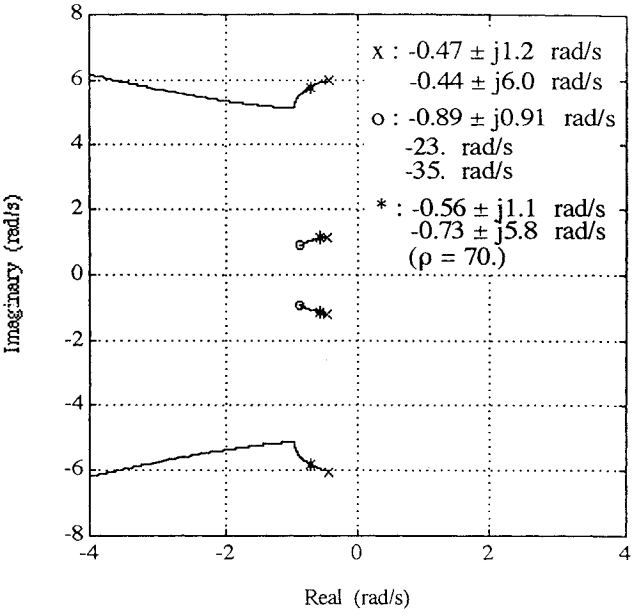


**Fig. 8 Closed-loop pole loci with parameter $\rho$.**

measurements to be used for feedback. The feedback measurements are the same as used for the conventional design, $q'$ and $q$. This selection leads to minimum-phase plant transmission zeros for the asymptotic loop transfer recovery algorithm, located at $-0.081$ and $-0.46\ s^{-1}$.

Figure 9 shows the resulting feedback compensators, prefilter stick gains, and closed-loop structure after the loop transfer recovery procedure is completed, and some straightforward pole-zero cancellations are performed on the compensators. Note the compensators consist of relatively simple lead-lag and lag-lead filters of second order. Table 3 contains the effective closed-loop transfer functions corresponding to the pilot command $\delta$, whereas Figs. 1–3 show the corresponding frequency responses. Short-period damping has improved from $\zeta_{sp} = 0.36$ to $\zeta_{sp} = 0.45$ (25% increase), whereas the first aeroelastic mode damping has improved from $\zeta_{f_1} = 0.073$ to $\zeta_{f_1} = 0.12$ (64% increase).

These improvements are also apparent in the closed-loop frequency responses. Besides improved short-period damping, the aeroelastic mode pole-zero sawtooth located near 6 rad/s in the angle-of-attack and pitch rate responses in Figs. 1 and 2 is reduced by roughly 10 dB when compared to the corresponding open-loop response. This is a result of improved closed-loop pole-zero cancellations (see Table 3), as desired in the model-following control synthesis (i.e., follow a rigid-body model). Note from Table 3 that the pole-zero cancellation here is not as precise as for the classical design. However, the model-following design may be fine tuned by considering nonequal relative weightings between $\alpha$ and $q$, or $\delta_E$ and $\delta_C$, in Eq. (15).

The two candidate control laws augment the aeroelastic effects by increased damping and improved mode cancellation. Only the former is effective when responses due to gust disturbances are of interest. If the present damping is not sufficient for acceptable gust response, then it will be necessary to increase the control law bandwidth by trading off some of the robustness margin to be discussed next.

## Robustness Analysis

Now consider the generic feedback loop structure in Fig. 10, which is a generalization of the closed-loop systems in Figs. 7 and 9, with response vector $y$, control inputs $u$, commands $y_c$, and plant, compensator, and prefilter transfer function matrices $G(s)$, $K(s)$, and $P(s)$, respectively. The feedback compensation in Fig. 10 is assumed to be synthesized with a design model $G(s)$, but the "true" plant transfer function is taken to be $G'(s)$.

Specifically, consider equal generic phase loss in each input channel to the plant, or

$$G'(s) = G(s)\{e^{-\tau s} I\} \tag{16}$$

This phase loss can represent, for example, unmodeled high-frequency dynamics originating from structural modes, actuators, sensors, structural filtering, computational delay, etc. Rewriting $G'(s)$ as

$$G'(s) = G(s)\{I + E(s)\} \tag{17}$$

it can be shown that

$$E(s) = (e^{-\tau s} - 1)I \tag{18}$$

where $E(s)$ is the so-called plant input multiplicative error.[4]

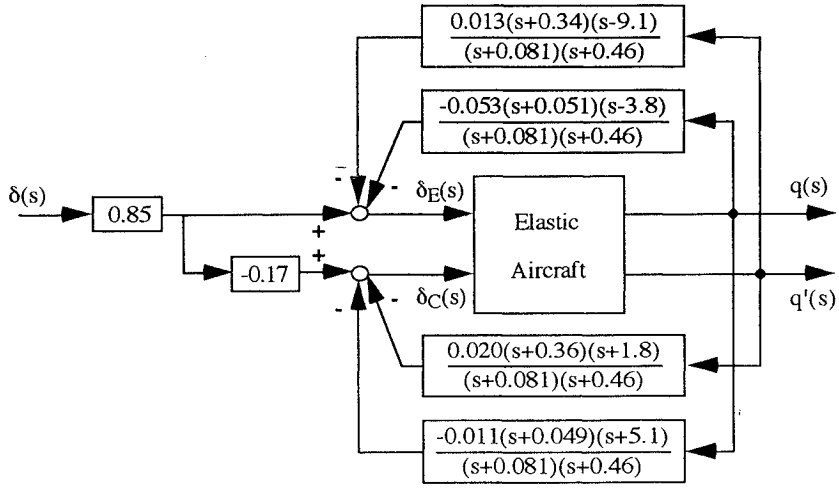


**Fig. 9 Model-following-designed closed-loop system.**

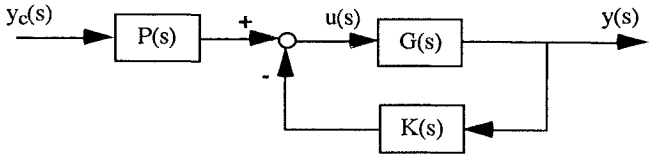


**Fig. 10 Generic multivariable closed-loop system.**

If the nominal closed-loop system is stable and the required number of encirclements of the critical point in Nyquist stability theory is the same for both nominal and true systems, then a sufficient condition guaranteeing closed-loop stability under $E(s)$ is[4]

$$\bar{\sigma}[E(j\omega)] < \underline{\sigma}[I + \{K(j\omega)G(j\omega)\}^{-1}] \qquad 0 \leq \omega \leq \infty \quad (19)$$

Here, $\underline{\sigma}$ and $\bar{\sigma}$ denote the minimum and maximum singular values, respectively. The "largest" value of $E(j\omega)$ for which Eq. (19) is satisfied gives a conservative indication of the system's multivariable stability robustness margin.

Figure 11 indicates the stability robustness of the classically designed closed-loop system, with the effect of multiplicative error due to generic phase loss in each input channel displayed as well. Note from Fig. 11 that the characteristic limiting the stability robustness is the dip in $\underline{\sigma}[I + \{KG\}^{-1}]$ near 6 rad/s. In fact, the phase loss allowed using this criterion is limited to $\tau \leq 0.3$ s. Figure 12 indicates the stability robustness properties of the model-following design, again with the effect of generic phase loss displayed. Note again a similar characteristic limiting the robustness of this feedback system. Here the allowable phase loss is $\tau \leq 0.35$ s, only slightly better than the previous result.

The question now turns to the genesis of this limiting characteristic. It is rather clear to correlate the limiting robustness characteristic in Figs. 11 and 12 with the augmented first aeroelastic mode in Table 3, since both occur at roughly 6 rad/s and structural modes limit robustness in precisely this manner. Therefore, any improvement in the damping of this mode should reduce this limiting characteristic. Beyond these general statements, very little definitive information is available concerning how the dominant aeroelastic mode parameters contribute to this characteristic, how the nearby short-period mode influences the situation, how the control system gains enter the problem, how the properties change with flight condition, how the sensor locations affect the characteristics, etc.

Insight into these issues is relevant to the flight control engineer, and to address them, an analytical analysis, similar to that presented in Ref. 13, is considered. Analytical expressions for $\underline{\sigma}[I + \{KG\}^{-1}]$ in terms of the closed-loop and open-loop properties exhibited by $KG$ will be developed. Further, analytical expressions for the vehicle transfer function poles and zeros in Table 2 and available from Refs. 10 and 11 will be used in the analysis.

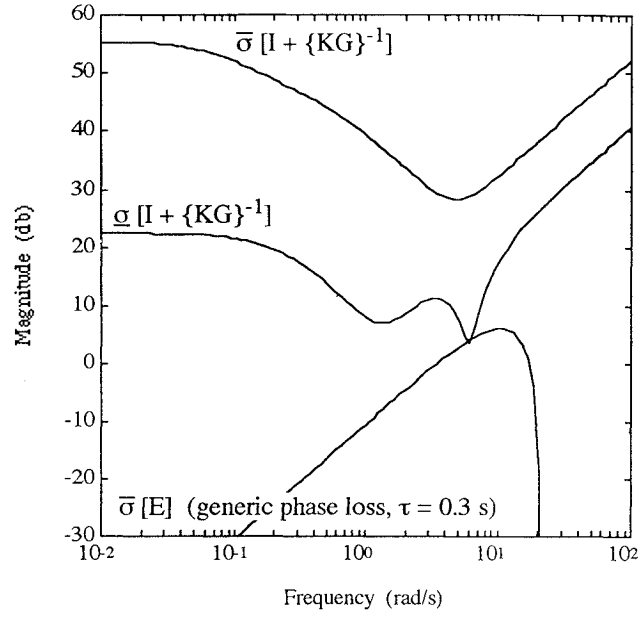


**Fig. 11 Classical design stability robustness analysis.**

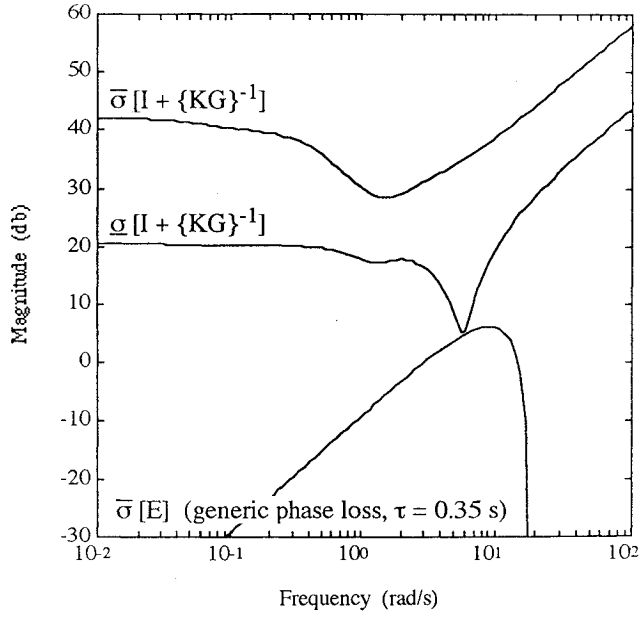


**Fig. 12 Model-following design stability robustness analysis.**

With reference to Fig. 10, consider a 2 × 2 closed-loop system with

$$K(j\omega) = \begin{bmatrix} k_{11} & k_{12} \\ k_{21} & k_{22} \end{bmatrix} \qquad G(j\omega) = \begin{bmatrix} g_{11} & g_{12} \\ g_{21} & g_{22} \end{bmatrix}$$
$$I + \{K(j\omega)G(j\omega)\}^{-1} = \begin{bmatrix} a_{11} & a_{12} \\ a_{21} & a_{22} \end{bmatrix} \tag{20}$$

where

$$\begin{aligned} a_{11} &= 1 + \frac{k_{21}g_{12} + k_{22}g_{22}}{\Delta} \\ a_{12} &= -\frac{k_{11}g_{12} + k_{12}g_{22}}{\Delta} \\ a_{21} &= -\frac{k_{21}g_{11} + k_{22}g_{21}}{\Delta} \\ a_{22} &= 1 + \frac{k_{11}g_{11} + k_{12}g_{21}}{\Delta} \\ \Delta &= \det[KG] = [k_{11}k_{22} - k_{12}k_{21}][g_{11}g_{22} - g_{12}g_{21}] \end{aligned} \tag{21}$$

The minimum and maximum singular values of $I + \{KG\}^{-1}$ are given as

$$\begin{aligned} \underline{\sigma}[I + \{KG\}^{-1}] &= \underline{\lambda}^{1/2}[(I + \{KG\}^{-1})(I + \{KG\}^{-1})^*] \\ \bar{\sigma}[I + \{KG\}^{-1}] &= \bar{\lambda}^{1/2}[(I + \{KG\}^{-1})(I + \{KG\}^{-1})^*] \end{aligned} \tag{22}$$

where $\underline{\lambda}$ and $\bar{\lambda}$ denote the minimum and maximum eigenvalues, respectively. Here, $\underline{\lambda}$ and $\bar{\lambda}$ solve

$$\begin{aligned} &\det[\lambda I - (I + \{KG\}^{-1})(I + \{KG\}^{-1})^*] \\ &\quad = \lambda^2 - (\underline{\lambda} + \bar{\lambda})\lambda + \underline{\lambda}\bar{\lambda} \end{aligned} \tag{23}$$

where

$$\begin{aligned} \underline{\lambda} + \bar{\lambda} &= |a_{11}|^2 + |a_{12}|^2 + |a_{21}|^2 + |a_{22}|^2 \\ \underline{\lambda}\bar{\lambda} &= |a_{11}a_{22} - a_{12}a_{21}|^2 \end{aligned} \tag{24}$$

If $\underline{\lambda} \ll \bar{\lambda}$, then, from Eq. (24), $\underline{\lambda}$ is approximately given as

$$\underline{\lambda} \approx \frac{|a_{11}a_{22} - a_{12}a_{21}|^2}{|a_{11}|^2 + |a_{12}|^2 + |a_{21}|^2 + |a_{22}|^2} \tag{25}$$

or

$$\underline{\sigma}[I + \{KG\}^{-1}] \approx \frac{|a_{11}a_{22} - a_{12}a_{21}|}{(|a_{11}|^2 + |a_{12}|^2 + |a_{21}|^2 + |a_{22}|^2)^{1/2}} \tag{26}$$

From inspection of Figs. 11 and 12, it can be seen that the condition $\underline{\lambda} \ll \bar{\lambda}$ (or $\underline{\sigma} \ll \bar{\sigma}$) is reasonably satisfied.

Substitution of Eq. (21) into the numerator and denominator of Eq. (26) yields

$$\begin{aligned} &|a_{11}a_{22} - a_{12}a_{21}| \\ &\quad = \left|\frac{1}{\Delta}\right| |1 + k_{11}g_{11} + k_{12}g_{21} + k_{21}g_{12} + k_{22}g_{22} + \Delta| \\ &|a_{11}|^2 + |a_{12}|^2 + |a_{21}|^2 + |a_{22}|^2 \\ &\quad = \left|\frac{1}{\Delta}\right|^2 (|k_{21}g_{12} + k_{22}g_{22} + \Delta|^2 + |k_{11}g_{12} + k_{12}g_{22}|^2 \\ &\qquad + |k_{21}g_{11} + k_{22}g_{21}|^2 + |k_{11}g_{11} + k_{12}g_{21} + \Delta|^2) \end{aligned} \tag{27}$$

These can be further simplified with the following observation[7]:

$$\begin{aligned} &1 + k_{11}g_{11} + k_{12}g_{21} + k_{21}g_{12} + k_{22}g_{22} + \Delta \\ &\quad = \det[I + KG] = \frac{\phi_{cl}}{\phi_{ol}} \\ &\Delta = \det[KG] = \frac{\psi_K\psi_G}{\phi_{ol}} \end{aligned} \tag{28}$$

where $\phi_{cl}$ and $\phi_{ol}$ denote the system's closed-loop and open-loop characteristic polynomials, respectively, and $\psi_K$ and $\psi_G$ are the compensator and plant transmission zero polynomials, respectively. With the notation

$$k_{ij}g_{pq} = \frac{n_{k_{ij}}n_{g_{pq}}}{\phi_{ol}} \qquad i, j, p, q = 1, 2 \tag{29}$$

where $n_{k_{ij}}$ and $n_{g_{pq}}$ denote the numerator polynomials of $k_{ij}$ and $g_{pq}$, respectively, substitution of Eqs. (27) and (28) into Eq. (26) yields the following analytical expression for $\underline{\sigma}[I + \{KG\}^{-1}]$:

$$\underline{\sigma}[I + \{KG\}^{-1}] \approx \frac{|\phi_{cl}|}{(|n_{11}|^2 + |n_{12}|^2 + |n_{21}|^2 + |n_{22}|^2)^{1/2}} \tag{30}$$

where

$$\begin{aligned} n_{11} &= n_{k_{21}}n_{g_{12}} + n_{k_{22}}n_{g_{22}} + \psi_K\psi_G \\ n_{12} &= n_{k_{11}}n_{g_{12}} + n_{k_{12}}n_{g_{22}} \\ n_{21} &= n_{k_{21}}n_{g_{11}} + n_{k_{22}}n_{g_{21}} \\ n_{22} &= n_{k_{11}}n_{g_{11}} + n_{k_{12}}n_{g_{21}} + \psi_K\psi_G \end{aligned} \tag{31}$$

Observe that the "zeros" of $\underline{\sigma}[I + \{KG\}^{-1}]$ are nothing more than the closed-loop poles, whereas the "poles" of $\underline{\sigma}[I + \{KG\}^{-1}]$ depend on the plant and compensator transfer function zeros as well as their transmission zeros. This result was first noted in Ref. 13, but the transmission zero polynomials $\psi_K$ and $\psi_G$ were related to the so-called coupling numerators.[5]

Now consider the classically designed closed-loop system shown in Fig. 7. Here

$$\begin{aligned} g_{11} &= q(s)/\delta_E(s) & k_{11} &= n_{k_{11}} = \delta_E/q \\ g_{12} &= q(s)/\delta_C(s) & k_{12} &= n_{k_{12}} = 0 \\ g_{21} &= q'(s)/\delta_E(s) & k_{21} &= n_{k_{21}} = \delta_C/q \\ g_{22} &= q'(s)/\delta_C(s) & k_{22} &= n_{k_{22}} = \delta_C/q' \\ \psi_G(s) &= -89(s + 0.081)(s + 0.46) & \psi_K &= k_{11}k_{22} - k_{12}k_{21} \end{aligned} \tag{32}$$

with $g_{ij}$ available from Table 2 and $k_{ij}$ available from Fig. 7. Substitution of the above quantities into Eq. (30) yields

$$\underline{\sigma}[I + \{KG\}^{-1}] \approx \frac{|(j\omega + 0.70 \pm j1.1)(j\omega + 0.75 \pm j6.0)|}{0.94|(j\omega + 0.22)(j\omega + 3.1 \pm j3.8)|} \tag{33}$$

It is evident from Eq. (33) that the augmented first aeroelastic mode poles, denoted

$$\begin{aligned} &s^2 + (2\zeta\omega)_{cl_2}s + (\omega^2)_{cl_2} = s^2 + 1.5s + 37 \\ &\quad = s + 0.75 \pm j6.0 \end{aligned} \tag{34}$$

and their low damping are directly responsible for the previously discussed critical stability robustness feature near 6 rad/s in Fig. 11.

From the classical design and Fig. 4, these poles are primarily a function of the $q'/\delta_C$ loop closure. With increasing $q'/\delta_C$ root locus gain $k_{22}$, these augmented aeroelastic mode poles originate from their open-loop locations

$$\begin{aligned} &s^2 + (2\zeta\omega)_{f_1}s + (\omega^2)_{f_1} = s^2 + 0.88s + 36 \\ &\quad = s + 0.44 \pm j6.0 \end{aligned} \tag{35}$$

and migrate toward their corresponding aeroelastic mode zeros in the $q'/\delta_C$ transfer function (see Table 2), denoted as

$$\begin{aligned} &s^2 + {}_{f_1}(2\zeta\omega)^{\delta_C}_{q'}s + {}_{f_1}(\omega^2)^{\delta_C}_{q'} = s^2 + 1.5s + 8.9 \\ &\quad = s + 0.73 \pm j2.9 \end{aligned} \tag{36}$$

yielding essentially the closed-loop locations in Eq. (34) for the selected value of $k_{22}$.

From Refs. 10 and 11, the open-loop natural frequency and damping terms of the aeroelastic mode poles and zeros in Eqs. (35) and (36) are approximately given by

$$(\omega^2)_{f_1} \approx \left(\omega_1^2 - F_{1\eta_1}\right) + \frac{(1 + (Z_q/V_{T_1}))M_{\eta_1}F_{1\alpha}}{(\omega_1^2 - F_{1\eta_1})}$$
$$= 35 + 2.0 \tag{37}$$

$$(2\zeta\omega)_{f_1} \approx (2\zeta_1\omega_1 - F_{1\dot{\eta}_1}) + \frac{M_{\eta_1}F_{1q} + \left[(Z_{\eta_1}/V_{T_1}) + (1 + (Z_q/V_{T_1}))M_{\dot{\eta}_1}\right]F_{1\alpha}}{\left(\omega_1^2 - F_{1\eta_1}\right)}$$
$$= 0.62 + 0.35$$

$$f_1(\omega^2)_{q'}^{\delta_C} \approx \frac{(\omega_1^2 - F_{1\eta_1})M_{\delta_C}}{M_{\delta_C} - \phi_1'(x)F_{1\delta_C}} - \frac{M_{\eta_1} + \phi_1'(x)(1 + (Z_q/V_{T_1}))M_\alpha}{\phi'_1(x)} \tag{38}$$
$$= 2.0 - (-6.5)$$

$$f_1(2\zeta\omega)_{q'}^{\delta_C} \approx \frac{(2\zeta_1\omega_1 - F_{1\dot{\eta}_1})M_{\delta_C} + \phi_1'(x)M_qF_{1\delta_C}}{M_{\delta_C} - \phi_1'(x)F_{1\delta_C}} - \frac{\phi_1'(x)(1 + (Z_q/V_{T_1}))(Z_\alpha/V_{T_1})M_\alpha F_{1\delta_C}}{(\omega_1^2 - F_{1\eta_1})M_{\delta_C}}$$
$$= 0.82 - (-0.67)$$

with the following numerical values:

$$\frac{Z_\alpha}{V_{T_1}} = -0.416\ \text{s}^{-1} \qquad 1 + \frac{Z_q}{V_{T_1}} = 1.03$$
$$\frac{Z_{\eta_1}}{V_{T_1}} = -0.00267\ \text{s}^{-1} \qquad M_\alpha = -3.33\ \text{s}^{-2}$$
$$M_q = -0.830\ \text{s}^{-1} \qquad M_{\eta_1} = -0.0655\ \text{s}^{-2}$$
$$M_{\dot{\eta}_1} = -0.00390\ \text{s}^{-1} \qquad M_{\delta_C} = 0.809\ \text{s}^{-2}$$
$$F_{1\alpha} = -1,040.\ \text{s}^{-2} \qquad F_{1q} = -78.4\ \text{s}^{-1}$$
$$F_{1\delta_C} = -631.\ \text{s}^{-2} \qquad (\omega_1^2 - F_{1\eta_1}) = 34.8\ \text{s}^{-2}$$
$$(2\zeta_1\omega_1 - F_{1\dot{\eta}_1}) = 0.621\ \text{s}^{-1} \qquad \phi_1'(x) = 0.0210\ \text{ft/ft} \tag{39}$$

The above parameters are the total flight velocity $V_{T_1}$, rigid-body and aeroelastic aerodynamic stability and control derivatives $Z_i$, $M_i$, and $F_{ij}$, first in vacuo elastic mode slope $\phi'_1(x)$ at the sensor location $x$, vibration frequency $\omega_1$, and damping ratio $\zeta_1$. These vehicle parameters appear explicitly in the linear equations of motion for the elastic aircraft[10,11] listed below:

$$\dot{\alpha} = \frac{Z_\alpha}{V_{T_1}}\alpha + \left(1 + \frac{Z_q}{V_{T_1}}\right)q + \frac{Z_{\eta_1}}{V_{T_1}}\eta_1 + \frac{Z_{\dot{\eta}_1}}{V_{T_1}}\dot{\eta}_1 + \frac{Z_{\delta_E}}{V_{T_1}}\delta_E + \frac{Z_{\delta_C}}{V_{T_1}}\delta_C$$
$$\dot{q} = M_\alpha\alpha + M_qq + M_{\eta_1}\eta_1 + M_{\dot{\eta}_1}\dot{\eta}_1 + M_{\delta_E}\delta_E + M_{\delta_C}\delta_C \tag{40}$$
$$\ddot{\eta}_1 = F_{1\alpha}\alpha + F_{1q}q - \left(\omega_1^2 - F_{1\eta_1}\right)\eta_1 - \left(2\zeta_1\omega_1 - F_{1\dot{\eta}_1}\right)\dot{\eta}_1 + F_{1\delta_E}\delta_E + F_{1\delta_C}\delta_C$$
$$q' = q - \phi_1'(x)\dot{\eta}_1$$

As seen from Eq. (37), the frequency of the open-loop aeroelastic mode poles is primarily due to the elastic mode structural frequency and aerodynamic stiffness (i.e., $\omega_1^2 - F_{1\eta_1}$). Also, the inherent low damping in this mode is primarily due to the elastic mode structural and aerodynamic damping (i.e., $2\zeta_1\omega_1 - F_{1\dot{\eta}_1}$). However, note also that approximately one-third of the total damping is due to aerodynamic coupling between the short-period and aeroelastic degrees of freedom. It is now clear which key vehicle and compensator parameters contribute to the critical stability robustness properties of this closed-loop system.

Now consider the model-following design closed-loop system shown in Fig. 9. Here

$$g_{11} = q(s)/\delta_E(s) \qquad k_{11} = \delta_E(s)/q(s)$$
$$g_{12} = q(s)/\delta_C(s) \qquad k_{12} = \delta_E(s)/q'(s)$$
$$g_{21} = q'(s)/\delta_E(s) \qquad k_{21} = \delta_C(s)/q(s) \tag{41}$$
$$g_{22} = q'(s)/\delta_C(s) \qquad k_{22} = \delta_C(s)/q'(s)$$
$$\psi_G(s) = -89(s + 0.081)(s + 0.46)$$
$$\psi_K(s) = -0.00091(s + 0.060)(s + 0.35 \pm j0.21)(s - 1.9)$$

with $g_{ij}$ available from Table 2 and $k_{ij}$ available from Fig. 9. Substitution of the above quantities into Eq. (30) yields

$$\underline{\sigma}[I + \{KG\}^{-1}] \approx \frac{|(j\omega + 0.56 \pm j1.1)(j\omega + 0.73 \pm j5.8)|}{0.66|(j\omega + 0.83 \pm j1.0)(j\omega + 4.6)|} \tag{42}$$

It is evident from Eq. (42) that again the augmented first aeroelastic mode poles

$$s^2 + (2\zeta\omega)_{\text{cl}_2}s + (\omega^2)_{\text{cl}_2} = s^2 + 1.5s + 34 = s + 0.73 \pm j5.8 \tag{43}$$

and their low damping are directly responsible for the critical stability robustness feature near 6 rad/s in Fig. 12. From the model-following design and Fig. 8, these poles originate at their open-loop location and migrate toward the plant transmission zeros (or their stable mirror image) defined through the model-following formulation as the control weighting in the loss function is reduced (or the loop gains are increased). Although literal approximations for these transmission zeros are unavailable, the expressions for the open-loop aeroelastic poles in Eq. (37) again reveal the major source of the critical stability robustness characteristics.

## Conclusions

Two different strategies for designing integrated flight and aeroelastic mode control laws have been successfully exercised. Both conventional and model-following-based techniques lead to closed-loop systems with roughly equivalent performance and stability robustness characteristics. However, the internal structure of the two control laws differ by having extra feedback channels present, having individual prefilter weights reversed, and having feedback channel sign differences. More important than these similarities and differences, both techniques allow the flight control designer to "see" how the control law augments the vehicle dynamics through the graphical root locus and to understand why the root loci are shaped a particular way via the "physics" for the conventional approach and via selection of the desired dynamics and followed responses for the model-following approach.

A numerical stability robustness analysis indicates that both closed-loop systems are limited by the damping of the augmented aeroelastic mode, and any improvement in this damping should lessen the constraint. Beyond this, however, very little additional, definitive results can be drawn from the numerical analysis. An analytical stability robustness analysis goes beyond this by offering insight concerning how the dominant aeroelastic mode parameters contribute to this characteristic, how the nearby short-period mode influences the situation, how the control system gains enter the problem, how the properties change with flight condition, how the sensor locations affect the characteristics, etc. This additional insight can be invaluable to the flight control engineer and would be more difficult to obtain from a strictly numerical analysis.

## Acknowledgments

This research was supported by NASA Langley Research Center under Grant NAG1-758. Doug Arbuckle and Carey Buttrill served as technical monitors.

## References

[1]Bisplinghoff, R. L., and Ashley, H., *Principles of Aeroelasticity*, Dover, New York, 1962.

[2]Waszak, M. R., and Schmidt, D. K., "Flight Dynamics of Aeroelastic Vehicles," *Journal of Aircraft*, Vol. 25, No. 6, 1988, pp. 563–571.

[3]Anderson, M. R., and Schmidt, D. K., "Formulating an Integrated Flight Control Law Synthesis Strategy," AIAA Paper 86-2711, Oct. 1986.

[4]Doyle, J. C., and Stein, G., "Multivariable Feedback Design: Concepts for a Classical/Modern Synthesis," *Transactions on Automatic Control*, Vol. AC-26, No. 1, 1981, pp. 4–16.

[5]McRuer, D., Ashkenas, I., and Graham, D., *Aircraft Dynamics and Automatic Control*, Princeton Univ. Press, Princeton, NJ, 1973.

[6]Blakelock, J. H., *Automatic Control of Aircraft and Missiles*, Wiley, New York, 1965.

[7]Kwakernaak, H., and Sivan, R., *Linear Optimal Control Systems*, Wiley, New York, 1972.

[8]Doyle, J. C., Glover, K., Khargonekar, P. P., and Francis, B. A., "State-Space Solutions to Standard $H_2$ and $H_\infty$ Control Problems," *Transactions on Automatic Control*, Vol. AC-34, No. 8, 1989, pp. 831–847.

[9]Pearce, B. F., Johnson, W. A., and Siskind, R. K., "Analytical Study of Approximate Longitudinal Transfer Functions for a Flexible Airframe," Aeronautical Systems Division, ASD-TDR-62-279, Wright-Patterson AFB, OH, June 1962.

[10]Newman, B., and Schmidt, D. K., "Numerical and Literal Aeroelastic-Vehicle-Model Reduction for Feedback Control Synthesis," *Journal of Guidance, Control, and Dynamics*, Vol. 14, No. 5, 1991, pp. 943–953.

[11]Newman, B., "Aerospace Vehicle Model Simplification for Feedback Control," Ph.D. Dissertation, School of Aeronautics and Astronautics, Purdue Univ., West Lafayette, IN, Aug. 1992.

[12]Livneh, R., and Schmidt, D. K., "New Literal Approximations for the Longitudinal Dynamic Characteristics of Flexible Flight Vehicles," *Proceedings of the AIAA Guidance, Navigation, and Control Conference* (Hilton Head, SC), AIAA, Washington, DC, 1992, pp. 536–545.

[13]McRuer, D. T., Meyers, T. T., and Thompson, P. M., "Literal Singular-Value-Based Flight Control System Design Techniques," *Journal of Guidance, Control, and Dynamics*, Vol. 12, No. 6, 1989, pp. 913–919.

[14]Newman, B., and Schmidt, D. K., "Multivariable Flight Control Synthesis and Literal Robustness Analysis for an Aeroelastic Vehicle," *Proceedings of the AIAA Guidance, Navigation, and Control Conference* (Portland, OR), AIAA, Washington, DC, 1990, pp. 1180–1189.

[15]Anderson, M. R., and Schmidt, D. K., "Error Dynamics and Perfect Model Following with Application to Flight Control," *Journal of Guidance, Control, and Dynamics*, Vol. 14, No. 5, 1991, pp. 912–914.